T2R2 東京科学大学 リサーチリポジトリ
Science Tokyo Research Repository

# 論文 / 著書情報
# Article / Book Information

| | |
|---|---|
| Title | Strength reduction of cohesionless soil due to internal erosion induced by one-dimensional upward seepage flow |
| Authors | Lin Ke, Akihiro Takahashi |
| Citation | Soils and Foundations, Vol. 52, Issue 4, pp. 698-711 |
| Pub. date | 2012, 8 |
| DOI | http://dx.doi.org/10.1016/j.sandf.2012.07.010 |
| Creative Commons | See next page. |
| Note | This file is author (final) version. |

Powered by T2R2 (Science Tokyo Research Repository)

# License


**Creative Commons:** CC BY-NC-ND

# Strength reduction of cohesionless soil due to internal erosion induced by one-dimensional upward seepage flow

Lin Ke[1] and Akihiro Takahashi[2]

**ABSTRACT**

Suffusion, one of the modes of internal erosion has been widely detected in both natural deposits and filled structures. It is the phenomenon that fine particles in soil gradually migrate through the voids between coarse particles leaving the soil skeleton. In this paper, the main focus is on soil strength change due to internal erosion. A series of one-dimensional upward seepage tests at constant water head is performed to cause internal erosion in a soil sample by controlling the three variable parameters, namely, (a) fine content and (b) relative density of the soil, and (c) maximum imposed hydraulic gradient in a sample. Mechanical consequences of the internal erosion are examined by the Cone Penetration Test. The internal erosion indicated by fine particle loss causes changes in void ratio and significant increase of hydraulic conductivity, resulting in decreasing in the soil strength from its initial value.

**Key words**: internal erosion; suffusion; upward seepage test; hydraulic conductivity change; strength reduction

**Soils and Foundations, 52(4), 698-711, 2012**
**Original URL:**
**http://dx.doi.org/10.1016/j.sandf.2012.07.010**

[1] PhD Candidate, Tokyo Institute of Technology
[2] Associate Professor, Tokyo Institute of Technology

## INTRODUCTION

Seepage-induced erosion, resulting from soil particle migration, is observed widely both in natural soil deposits and artificial engineered fill structures. The most significant influence of seepage erosion is on earth dams, the failure of which due to internal erosion could have catastrophic consequences. The gap-graded cohesionless soil is especially vulnerable to internal erosion due to its deficiency in certain particle size. This kind of material has played a significant role in the potential for seepage induced internal erosion.

In literature, the term "internal erosion" usually refers to the detachment of soil particles from main soil structures due to mechanical or chemical action of a fluid flow. The "internal erosion" customarily contains "suffusion" and "piping" phenomenon. In suffusion, the fine particles are eroded through the voids between the larger particles by seepage flow leaving the coarse skeleton, while the progressive erosion and transportation of soil particles along a flow path indicate the phenomenon of piping. They may lead to the obvious changes of porosity, significant increase of hydraulic conductivity and potential reduction of soil strength. Suffusion and piping are always coupled phenomenon. The common term "internal erosion" is used here to describe the target phenomenon that small particles are washed out through the voids between the coarse particles by seepage flow leaving the soil skeleton.

The hydrological mechanism of internal erosion has been widely investigated. The hydraulic gradient change (critical hydraulic gradient), hydraulic conductivity change and fine particle loss were the primary concern. The initial systematical experimental investigation was the base soil and filter compatibility studies (Terzaghi and Peck, 1948; US Army Corps of Engineers, 1953; Istomina, 1957; Kenney and Lau, 1985, 1986; among others). By recognizing the effective particle size ratio between the base soil and filter, many empirical

methods, namely geometrical criteria, were proposed to prevent soil erosion and allow for water seepage. The phenomenon that base soil or filter, that satisfies the geometrical criteria, could fail because of internal erosion of fine particles led to the soil internal instability studies (Skempton and Brogan, 1994; Tomlinson and Vaid, 2000; Moffat and Fannin, 2006; among others). In those experimental investigations, not only the soil geometric characteristics, but also the influence of other factors on internal erosion has been considered, such as flow velocity, flow direction and hydraulic gradient. Tested soil were those "poor graded" soils, which means gap-graded or coarse widely graded soils. The main apparatus usually contained a permeameter together with the measurement of pore water pressure to characterize hydro-mechanical spatial variations and vertical load to obtain the effective stress distribution along the specimen. The particle erosion rate and possible chemical reactions, if any, were also measured.

The internal erosion occurs if the following criteria are satisfied (Wan, 2006): (a) the size of the fine particles is smaller than the size of the void between coarse particles which form the skeleton of the soil and the amount of fine particles is less than enough to fill the voids between coarse particles (geometrical criteria); (b) The hydraulic gradient is large enough to move the fine soil particles through the void between coarse particles (hydraulic criterion).

The hydro-mechanical properties of soil, such as internal erosion onset hydraulic gradient, may closely relate with fine content. Experimental research also has indicated that change in fine content may cause either decreasing or increasing of soil strength. The soil behavior seems to be dependent on the range of fine content, which may be the possible reason to explain the soil strength change after internal erosion. Due to the difficulties in explaining fine content dependent soil behavior by "void ratio" concept alone, Thevanayagam and Mohan

(2000) proposed "intergranular void ratio" by assuming that the volume of fines is a part of the voids between coarser particles. If the differences in specific gravity of the coarser and finer particles are neglected, the "intergranular void ratio, $e_s$" could be obtained from void ratio and fine content. On the basis of a demarcation line corresponding to $e_s=e_{max,HS}$ (Maximum void ratio of coarse particles), the soil behavior depending on the combination of void ratio and fine content is divided into three cases (cf. Fig. 4 appears later): Case 1 is at relatively smaller void ratio with the smaller fine content. In this case, the intergranular void ratio of the soil specimen is smaller than the maximum void ratio of coarse particles. Most of the fines are locked in the intergranular voids. The soil behavior largely depends on the coarse materials. Case3 is at relatively larger void ratio. The intergranular void ratio is larger than the maximum void ratio of coarse particles. In this case, coarse particles are separated by the fines, leading to a relatively unstable soil structure. The shear strength of the soil could be significantly influenced by the shear resistance along the fines. Case2 is at the intermediate void ratio. The intergranular void ratio is approximately equal to the maximum void ratio of coarse particles. The anticipated soil behavior would depend on whether or not the fines are locked in the intergranular voids or work as separators between coarse particles. Vallejo (2001) explained the strength change of binary mixtures by porosity and the mixture structure. The soil structure is characterized by coarse particles when the coarse particle concentration is greater than 70% while the fine particles dominated if the coarse particle concentration is less than 40%. In between them, both coarse and fine particles partially characterize the soil structures. The shear strength of a binary mixture is directly influenced by the frictional strength between the particles which hold the structures. To shed light on the strength-deformation properties of binary mixtures, Omine (1992, 1996) proposed a two-phase mixture model. In this model, a new parameter, corresponding to the volume content of fines, is introduced to evaluate stress distribution in mixtures. By assuming that strain energy

increments of fines and matrix per unit volume are equal, incremental stress-strain relationship of mixtures could be derived based on the new parameter. The validity of this model is confirmed by the unconfined compression test results of the mixtures of expanded polystyrol and kaolin clay. It is found that the unconfined compression strength of the mixtures decreases with the increase in the volume content of expended polystyrol pieces.

The primary purpose of this study is to evaluate the soil strength reduction after internal erosion. The hydraulic conditions which trigger internal erosion with reference to the influence of fine particle content, relative density and imposed hydraulic gradient are obtained by a series of upward seepage tests. A multi-stage test procedure is conducted to assess the condition necessary to trigger the internal erosion. Strength change of the soil subjected to internal erosion is evaluated by cone tip resistance profile from Cone Penetration Test (CPT).

## UPWARD SEEPAGE TEST

### *Tested material*

According to the previous studies, a soil with "fine fraction" and "coarse fraction" is vulnerable to internal erosion. The binary mixtures in this study consist of two Silica sands (Silica No.3 and No.8) having different dominant particle sizes. With larger particle size, the Silica No.3 works as the coarse particles while the fine Silica No.8 is the erodible fine particles. The siliceous sand used is mainly composed by quartz, categorized as angular to sub-angular material. Particle size distribution, specific gravity, maximum and minimum void ratios, and hydraulic conductivity, are summarized in Fig. 1, Tables 1 and 2.

### *Test specimens*

Primary target of seepage tests is to create internally eroded saturated soil specimens. To this end, the initial condition of those test specimens has to meet the criteria of onset of internal

erosion mentioned above. The geometrical criteria could be satisfied if the phase relationship between the coarse particles and the fine particles, shown in Fig. 2, are considered.

The mass balance of the soil can be expressed as:

$$f_s + f_f = 1 \quad \ldots\ldots\ldots (1)$$

where $f_s$ is the mass ratio of the coarse particles, equaling to $W_s/(W_s + W_f)$ and $f_f$ is the mass ratio of the fine particles, equaling to $W_f/(W_s + W_f)$.

Assume all the fine particles are erodible, and then the coarse particle void ratio is

$$e_s = (V_w + V_f)/V_s \quad \ldots\ldots\ldots (2)$$

and the fine particle void ratio is

$$e_f = V_w/V_f \quad \ldots\ldots\ldots (3)$$

From Eqn. (1), (2) and (3) with assumption that specific gravity of coarse and fine particles is the same, the following equation is obtained:

$$f_f = e_s/(1 + e_s + e_f) \quad \ldots\ldots\ldots (4)$$

Equation (4) indicates that the possible maximum value of $f_f$ is reached in an ideal condition: the coarse particles in a binary mixture specimen are loosely packed, while the fine particles are densely packed inside the voids between the coarse particles. Since the maximum void ratio of No.3 sand is 1.009 (the primary fabric formed by Silica No.3 is loosely packed) and the minimum void ratio of Silica No.8 is 0.703 (the fine particles, Silica No.8, are densely packed), the possible maximum mass ratio of erodible fines is 37%. A series of four binary mixtures is determined as test soils based on the above calculation. The fine content of the four mixtures is 25%, 20%, 16.7% and 14.3% respectively, less than the calculated possible maximum value. The particle size distributions, the specific gravity, maximum and minimum void ratios of the four tested soils are shown in Fig. 3 and Table 3.

To ensure the internal erosion would occur during the seepage test, the vulnerability of the four mixture soils to internal erosion is assessed by five currently available methods proposed by U.S.Army Corps of Engineers (1953), Istomina (1957), Kenney and Lau (1985, 1986), Burenkova (1993) and Mao (2005). The results are summarized in Table 4. The four soils are potentially unstable and vulnerable to internal erosion if seepage takes place.

*Selection of relative densities of specimens*

A plot of void ratio against fine content is shown in Fig. 4. The demarcation line, located between the maximum and minimum void ratio line, is determined by $e_s=e_{max,HS}$ (Thevanayagam and Mohan, 2000), where the intergranular void ratio $e_s$ is defined as:

$$e_s = \frac{e + FC}{1 - FC} \quad \text{..... (5)}$$

$e$ is the soil void ratio and $FC$ is fine content. The soil behavior around this line may be influenced by both coarse particles and fines. If those fines which actively play a role in transferring loads are eroded, the soil strength may be changed accordingly. In this series of tests, relative densities of the specimens are expected to cover this demarcation line. Two different relative densities are finally selected for each soil specimen as shown in Fig. 4 and Table 5.

*Test apparatus*

Constant head seepage tests with upward water flow are performed to cause internal erosion. A schematic diagram of the seepage test apparatus is shown in Fig. 5. The cylindrical seepage cell is 100mm in internal diameter and 300mm in height. The transparent seepage cell allows the observation of internal erosion from side. The upper end of the seepage cell is left open so that the erosion process can be observed from the top. An overflow pipe is fitted at the top

portion of the seepage cell to manually measure the flow rate by a cylinder. Two 10mm thick plastic rings with waterproof tape are set separately on the top and at the bottom of the specimen to prevent the formation of large seepage channels between the soil and side wall. The layer consisting of 2mm single-sized glass balls underneath the 170mm thick specimen serves to break up the incoming flow to ensure uniform water flow on the specimen. Nonwoven textile is placed at the bottom of the specimen to prevent downward fine particle loss. Water head variation within the specimen is measured by four stand pipes at four different depths: 20mm, 50mm, 105mm and 165mm. The inlet is connected with a constant water head tank which can be raised or lowered to control the hydraulic gradient across the specimen while the outlet is open to atmosphere.

*Specimen preparation*

To prevent the segregation of the two different sized particles, moist tamping method is employed (Ladd, 1978; Frost and Park, 2003). This method achieves uniform specimens by the concept of "undercompaction": each layer is compacted to a lower density than the desired value by a predetermined amount because of the fact that the compaction of succeeding sand layers would also densify the layers below. It is proved to be reliable by other scholars (Bradshaw and Baxter, 2006; Yang et al, 2008). The sample preparation procedures are as follows: determine the oven-dried weights of both Silica No.3 and No.8 for a test according to the prescribed fine content and relative density. Adjust the water content to an appropriate value. Usually, for the larger fine content specimen, larger water content is preferred (e.g. the initial water content of Specimen A is 8% while that of Specimen D is 5%). Thoroughly mix the soils with water to make the fine particles distributed as uniformly as possible. This procedure is usually done at least 16 hours before use. The specimen is prepared layer by layer. Weigh the amount of material required for each layer, and place it

into the cell by scoop. A tamping rod is used to compact the soil to the required height determined by "undercompaction". Upon completion, weigh the specimen to check the relative density again and record. This process usually takes two hours. Saturation of the specimen is performed in a vacuum tank. De-air water is purged into the specimen from the bottom inlet at a slow rate. This process approximately takes 5 ~ 6 hours to ensure the saturation quality.

*Test procedure*

A series of tests is conducted following a multi-stage procedure. Each test usually takes 5 ~ 6 hours depending on the imposed hydraulic gradient. The detailed test procedures are as follows:

(1) Before test, check the position of water level of the four standpipes to make sure the initial water head is the same. The level of constant water head tank is adjusted to ensure its water table is the same as that of the seepage cell.

(2) The initial imposed hydraulic gradient is usually in the range of 0.05~0.1. Increase the hydraulic gradient at the approximately same increment. When the hydraulic gradient reaches around the value required to cause initial internal erosion, the increment could be relatively smaller.

(3) For each step, allow 30 minutes to ensure the completion of the internal erosion, i.e., discharge rate is stable and the effluent color becomes clear. Record the water head distribution from the stand pipes. Estimate the discharge rate by measuring the volume of discharge effluent per minute for three times. Record the water temperature. Carefully observe the phenomenon occurring during the test, such as the flow turbidity, the jumping, piping or transportation of the fine particles and record them by camera.

(4) Repeat (2) and (3) until the soil becomes unstable, e.g. the specimen shows "boiling", or until the largest achievable hydraulic gradient is imposed if instability does not occur.

## UPWARD SEEPAGE TESTS RESULTS AND DISCUSSION

### *Definitions*

Two types of critical hydraulic gradients are presented:

Critical hydraulic gradient for soil stability $i_c$ was proposed by Terzaghi to determine a zero effective stress condition. It is related with the void ratio and the specific gravity of soil particles. It always accompanies with the phenomenon of "boiling" or "heaving" of both the coarse and fine particles. For cohesionless soils, $i_c$ is approximately equal to 1.

Critical hydraulic gradient for internal erosion, $i_s$ corresponds to the minimum hydraulic gradient at which the first sign of internal erosion appears when the imposed hydraulic gradient gradually increases, indicated by slight rushing out of fine particles. It corresponds to the inflection point in the hydraulic gradient and flow velocity relationship curve.

### *Observed fine particle migration*

All the test specimens except Specimen D-30 showed internal erosion phenomenon. The hydraulic behavior of those specimens, such as the tendency of flow velocity and hydraulic gradient relation, is similar. Since the phenomenon observed in Specimen A is obvious and typical, the results of Specimen A are mainly showed after in the paper for discussion. Figure 6 shows the observation of the fine particle loss from the top (Specimen A-30). Before onset of the internal erosion, the fine particles stay still. When the critical hydraulic gradient for internal erosion is reached, small "dancing-like" movement of fine particles occurs. A very

light layer of sand silk is covered on the top surface. Then a few sand spots or sand volcanoes appear after increasing the hydraulic gradient. Slight movement of fine particles is found around those spots. At the larger imposed hydraulic gradient, the number of the sand spots becomes more covering the whole area and the movement of fine particles around those spots is fiercer. As the hydraulic gradient is further increased, a piping-like phenomenon happens.

*Onset of internal erosion*

The typical relationship between hydraulic gradient and flow velocity (Specimen A-30) is shown in Fig. 7. At first, the approximate linear relationship between hydraulic gradient and flow velocity, in accordance with Darcy's law indicates no internal erosion occurs. At this stage the effective porosity representing the porosity available to contribute to fluid flowing through the specimens stays basically the same irrespective of the hydraulic gradient. After reaching the critical hydraulic gradient for internal erosion $i_s$, the curve slope begins to inflect, corresponding to the first observation of "dancing-like" movement of fine particles. The fine particles are washed out by the seepage flow, leading to the increasing of effective porosity and thus hydraulic conductivity. It can be inferred that when the critical hydraulic gradient for soil stability $i_c$ is reached, the "heaving" phenomenon occurs and the specimen reaches the state of zero effective stress.

*Hydraulic conductivity*

Since the amount of the fine particle loss varies with the depth, the hydraulic conductivity is not uniform along depth. In this section, local hydraulic conductivity change is calculated by the local hydraulic gradient assuming that the seepage flow obeys the Darcy's law. Figure 8 shows the relationship between average hydraulic gradient and local hydraulic conductivity of each layer for Specimen A-30.

Before internal erosion ($i$ < 0.13), slight increasing of the hydraulic conductivity with the imposed hydraulic gradient could be observed because of the nature of the upward seepage flow test: the upward flow would decrease the effective stress, similar to unloading the soil, and void ratio will correspondingly increase, leading to the increasing of hydraulic conductivity even without internal erosion. However, comparing to the drastic increment of hydraulic conductivity due to the loss of fine particles, the hydraulic conductivity is thought to be basically constant before internal erosion and its increment could be negligible. After the onset of the internal erosion, the hydraulic conductivity obviously increases with the imposed hydraulic gradient, resulting in 3 times of the initial value when the maximum imposed hydraulic gradient of 0.22 is reached. The loss of fine particles would lead to the increasing of hydraulic conductivity.

*Influence of controlled factors*

Figure 9 shows the variance of the critical hydraulic gradient for soil stability and the critical hydraulic gradient for internal erosion with the different initial fine content for the dense soil specimen (60% relative density). The calculated critical hydraulic gradient for zero effective stress following Terzaghi's equation are 1.08, 1.06, 1.05 and 1.03 and the experimental values of critical hydraulic gradient for internal erosion are 0.21, 0.23, 0.24 and 0.25, respectively. It is in accordance with the test results of Skempton and Borgan(1994): in the unstable materials migration and strong piping of fines takes place at gradients of about one fifth to one third of the theoretical value. There seems to be a trend that the specimen with less fine content requires a larger hydraulic gradient to cause internal erosion. The loose specimens also show the same trend (Fig. 10).

The influence of relative density on critical hydraulic gradient for internal erosion is presented in Fig. 11. A larger relative density for the specimen with the same fine content leads to a larger value of critical hydraulic gradient for internal erosion.

*Fine particle loss during internal erosion*

Typical post test particle size distribution curves of each zone (Fig. 5) of the Specimen A-60 at $i_{max}$ = 0.45, are shown in Fig. 12. The distribution curve of each layer after internal erosion shifts downward from original curve after internal erosion, indicating there is fine particle loss. The extent of the movement proportionally increases with the amount of fine particle loss. A graphical method proposed by Kenney and Lau (1985) is used to approximately assess the fraction of eroded fine particles as well as the largest eroded fine particles based on the change in the particle size distribution curve. A detailed calculation is shown in Fig. 13. The main idea of this method is to extend the initial particle size distribution curve of the test sample to match the curve after internal erosion. Since the coarse particles stay the same after internal erosion, by extending the vertical scale of the initial particle size distribution curve, the coarse part of the initial curve should match that of the post test particle size distribution curve. The fraction of eroded fine particles could be calculated from the amount of the movement of the initial particle size distribution curve.

Table 6 presents the particle loss (percentage of total mass) after imposing two different maximum hydraulic gradients for Specimen A-60. It is noted that the fine particle loss of the bottom layer is the most since the bottom layer has no “fine particle supply”. The fine particles are washed away leading to a large amount of particle loss. For the middle and upper layer, although their fine particles are washed away by seepage flow, the fine particles from the bottom layer are dragged up by seepage flow, forming a particle supplement to those

layers. Due to the open-ended nature of a water channel, more particles will be eroded from top layer comparing to middle layer. This finding is in accordance with Kenney and Lau (1985). They defined the three layers as a top transition zone, a central homogeneous zone and a bottom transition zone, respectively. The particle loss in top and bottom zone is larger than central zone.

For Specimen A-60, B-60 and C-60, different maximum hydraulic gradients larger than critical hydraulic gradient for internal erosion are imposed to find its influence on fine particle loss. Relationship between the maximum imposed hydraulic gradient and fine particle loss of those specimens with different fine content are shown in Fig. 14. There is a general trend that the larger the maximum imposed hydraulic gradient, the larger the fine particle loss. Specifically, before onset of the internal erosion, the soil specimens are stable without any fine particle loss. Once internal erosion starts, the particle loss increases with the imposed hydraulic gradient. At the same imposed hydraulic gradient, the specimen with larger fine content shows more erosion potential. Due to the relatively large hydraulic conductivity of the tested specimens, the hydraulic gradient, greater than 0.51, cannot be imposed. Since the amount of erodible fine particles in a mixture is definite, the eroded fine particles would not increase unlimitedly with the imposed hydraulic gradient. When certain hydraulic gradient is reached, the fine particle loss would close to its limit and be stable irrespective of hydraulic gradient.

*Void ratio and volumetric deformation*

An obvious characteristic of internal erosion is the soil microstructure change, resulting in the increasing of void ratio and volumetric deformation. Due to the nature of the upward seepage tests, precise measurement of soil deformation during seepage tests could not be conducted.

By observation, there is a trend that after internal erosion, the tested specimen subsides (Fig. 15). The largest deformation is observed at Specimen A-60. The volumetric strain caused by internal erosion is about 6%. The specimen deformation is caused by both the soil particles loss and possible voids change due to the soil particle spatial adjustment, as is shown in Fig.16. The largest increasing of void ratio occurs if there is no deformation during the internal erosion, corresponding to the Mitchell (1976) assumption that the fine particles occupy the voids between coarse particles and may not participate in the force transfer. The loss of those fines would not cause any deformation in the soil fabric. The minimum volumetric strain is 0. However, in practice, the internal erosion would always accompany with the deformation of soil structure, which is regarded as a sign of instability. It may be better to consider this possibility as an ideal simplification in theory. The minimum void ratio of the specimen after erosion could be estimated by the greatest compaction that the coarse particles could achieve, resulting from the soil particle rearrangement. Under this circumstance, the volumetric deformation of the specimen would reach the maximum value.

The soil volumetric deformation is accompanied by the possible loss of those fines actively engaged in mechanical transfer and the spatial rearrangement of soil particles, both of which would probably adjust the force transfer path in specimens and consequently, lead to the soil strength reduction after internal erosion.

## CONE PENETRATION TEST (CPT)

Due to the difficulties in retrieving undisturbed samples from the seepage cell after the tests, an in-situ testing technique is needed to characterize the mechanical properties of the specimen. The miniature Cone Penetration Test (CPT) was selected because it offers

continuous measurement of cone resistance along depth and excellent repeatability. In practice, the friction angle of sand deposits can be estimated from the results of CPTs (Terzaghi, Peck and Mesri, 1996). By conducting CPT before and after the application of seepage flow to the specimen, the strength reduction due to the internal erosion can be evaluated. The miniature cone used in the tests is a cylindrical cone tip with the diameter of 10mm and 60° tip apex angles (Fig. 17). By using an embedded load cell, resistance at the tip can be measured. A jack is connected to the upper end of the penetrometer to push the cone into specimens by constant rate. Data acquisition system allows automatic cone tip resistance recording. Penetration rate is 20 mm/sec, following the JGS 1435-2003. Total penetration depth is 160mm. According to Been, et al (1986) who reviewed the problems associated with calibration chamber test, size effect, including particle size and chamber size effect, and boundary effect are the most important issues. The diameter ratio of seepage cell to cone in this research is 10, which might cause size effect. Some assessments on the size effect in this study could be found in appendix. All the test specimens are listed in Table 7.

*Cone resistance profile*

Profiles of the cone tip resistance for Specimen A, B, C and D at 60% relative density are shown in Fig. 18. A larger fine content leads to a smaller cone tip resistance. A potential explanation is that for the gap-graded soil, coarse particles work as the soil skeleton and the interlocking between them are primary. The fine particles work as separators between coarse particles. With more fine content, those “separators” decrease the frictional forces between coarse particles, resulting in a smaller shearing resistance and, correspondingly, decreasing the cone tip resistance.

The influence of internal erosion on CPT is demonstrated by the cone tip resistance profiles obtained before and after internal erosion. As an example, those of Specimen A-60, are shown in Fig. 19. After internal erosion, the cone resistance decreases indicating that the internal erosion process may have changed the interlocking of soil particles leading to the cone resistance decreasing. However, the strength reduction may potentially be induced by either fine particles loss, weakening soil particle interlocking or size effect. In previous researches, the size effect is closely related with soil relative density. As the relative density is not so large (60% maximum) it can be said that the resistance reduction is mainly caused by the fine particle loss rather than size effect.

Figure 19 also reveals that the cone tip resistance reduction has certain relationship with the maximum imposed hydraulic gradient. Before internal erosion, the soil structure is assumed to keep constant irrespective of hydraulic gradient. After the onset of the internal erosion, the larger the maximum hydraulic gradient imposed, results in the more the fine particle loss and therefore, further cone tip resistance reduction.

*Cone resistance interpretation*

The CPTs data are interpreted into a mechanical parameter to make the CPT results easier to understand from engineering point of view and compare with different cases. The approach of the interpretation is to develop empirical correlations between cone tip resistance and behavioral properties of soils (e.g. angle of shearing resistance) based on various theories. Cone tip resistance is the measurement of CPTs and behavioral properties of soils are obtained from laboratory test. The most practical model explaining the cone tip resistance is the Bearing capacity theory, on the basis of limit equilibrium method, proposed by Terzaghi (1948). This method assumed the failure mechanisms and then determined the failure load by

assuming that the soil is a rigid-plastic material. However, it was criticized by taking no account of soil compressibility, leading to unreliable predictions of angle of shearing resistance (Vesic, 1972). However, Janbu and Senneset (1974) reported a relationship between bearing capacity number $N_q$, the ratio of cone resistance $\Delta q_c$ and vertical effective stress $\Delta\sigma_v'$, and angle of shearing resistance with little data scattering which indicated the limited influence of soil compressibility. Work by Al-Awkati (1975) further proved for quartz sands, compared to compressibility, shear strength had more influence on cone resistance and therefore, the bearing capacity theory could provide reasonable prediction. For silica sand, it is reasonable to empirically correlate the bearing capacity number ($N_q$) derived from CPT and the drained angle of shearing resistance ( $\phi'$ ), which may be commonly represented as following:

$$\tan\phi' = A_1 + A_2 \ln(\Delta q_c / \Delta\sigma_v') \quad \ldots\ldots\ldots (6)$$

where $\Delta\sigma_v'$ is the vertical effective stress increment at the depths where the cone tip resistance increment $\Delta q_c$ is measured ( $N_q = \Delta q_c / \Delta\sigma_v'$ ). $A_1$ and $A_2$ are regression coefficients. Durgunoglu and Mitchell (1975) initially proposed a design chart to determine the angle of shearing resistance based on bearing capacity theory. The curve-fitting yields $A_1$= 0.215 and $A_2$=0.131. This method is found applicable for the sands with low compressibility. Based on the calibration chamber test results on normally consolidated, moderately compressible, predominantly quartz sands, Robertson and Campanella (1983) showed a correlation in the form of a design chart and the regression coefficients are $A_1$= 0.194 and $A_2$=0.147.

Following the common calibration procedure, the interpretation is performed to compare the measured cone penetration resistance, in terms of $N_q$, and the measured angle of shearing resistance from direct shear box test. Since the tested specimens (A, B, C, D) mainly consist

of Silica No.3, the frictional forces of which are primary in shear strength, several fully saturated specimens consisting of solo Silica No.3 sand, are tested as well for calibration purpose. Those cases correspond to the extreme consequences of erosion: all the fines are eroded. Details are given in Table 8. The calibration chamber is the same as used in seepage tests.

To avoid possible bottom boundary effects, the cone resistance data of 30mm~100mm depth are selected to evaluate bearing capacity number $N_q$. The bearing capacity number obtained from the cone resistance profile (Fig.18) of Specimen A, B, C and D at 60% relative density are shown in Table 8. Being the same as cone tip resistance, bearing capacity number also decreases with fine content. The bearing capacity number could be thought as the mechanical parameter which could characterize the cone tip resistance. The reduction of the bearing capacity number due to internal erosion could be seen from Fig.19. After internal erosion, the bearing capacity number decreases and the extent of bearing capacity number decreasing seems to be dependent on the imposed hydraulic gradient. This trend could be clearly noted from Fig. 20, which shows the relationship between the maximum imposed hydraulic gradient and normalized bearing capacity number (The ratio of bearing capacity number after and before internal erosion). For Specimen A-60, after internal erosion at the hydraulic gradient of 0.45, the bearing capacity number $N_q$ decreases by approximately 30% while at the hydraulic gradient of 0.54, $N_q$ deceases by about 70%.

The angles of shearing resistance of tested specimens are obtained by conducting constant pressure Direct Shear Box Tests. The apparatus consists of shear boxes, guide for the shear box and loading system for both vertical force and shear force. The soil specimens are prepared by moist tamping method, ensuring the similar soil condition as in seepage tests.

Each tested specimen is subjected to shearing at the velocity of 0.2 mm/min, following JGS 0560-0561, to allow volume change of the specimen while the effective normal stress on the shear plane is maintained at a constant value. For the same specimen, four different normal stresses, 25kPa, 50kPa, 100kPa and 200kPa, respectively are conducted. A typical shearing result of Specimen A-60 is shown in Fig.21.

The comparison between the bearing capacity number from CPT data and angle of shearing resistance obtained from direct shear box test is shown in Fig. 22. Due to the influence of compressibility, there is some scattering in the results. The best fitting curve by Logarithmic function are shown in Eq. (7).

$$\tan\phi' \approx 0.573 + 0.1\ln(\Delta q_c / \Delta\sigma_v') \quad \ldots\ldots\ldots \quad (7)$$

Since this empirical correlation compares two different shear modes, i.e., simple shear in the direct shear box and compression at the cone tip, it would underestimate the angle of shearing resistance value due to the influence of compressibility (Robertson and Campanella, 1983) and therefore, the strength reduction index in terms of $\tan\phi'$ may not reflect the actual strength reduction quantitatively. However, at least, it may shed light on how the internal erosion affects the strength parameter in general.

To make the comparison clear, the strength reduction is defined as following based on this correlation:

$$\Delta R = 1 - \frac{\tan\phi'_{\text{post-erosion}}}{\tan\phi'_{\text{before-erosion}}} \quad \ldots\ldots\ldots \quad (8)$$

where $\Delta R$ is the strength reduction by percentage after erosion; $\phi'_{post-erosion}$ is the angle of shearing resistance after internal erosion and $\phi'_{before-erosion}$ is the angle of shearing resistance before internal erosion.

The soil strength change due to internal erosion for both the loose and dense specimens is summarized in Table 9. After internal erosion, the cone tip resistance decreases, resulting in the decreasing of the estimated angle of shearing resistance. Depending on the imposed hydraulic gradients, the fine particle loss is different. The relationship between the maximum imposed hydraulic gradient and normalized soil strength (1-$\Delta R$) is shown in Fig. 23. The larger imposed hydraulic gradient causes further soil strength reduction. Up to the imposed hydraulic gradient of 0.5, strength change is gentle, while drastic change can be seen with the imposed hydraulic gradient over 0.5. However, the fine particle loss does not increase with the imposed hydraulic gradient unlimitedly. Due to the limitation of the system, authors could not impose large hydraulic gradient to the samples. However, it could be inferred that at certain stage, the particle loss may be constant irrespective of the imposed larger hydraulic gradient. Correspondingly, an upper limit of soil strength reduction due to internal erosion may exist, as shown in Fig. 24. It is worth to mention that the hydraulic gradient referred here is within the range between $i_s$ and $i_c$. Out of this range, the soil may be stable or fail.

## CONCLUSIONS

Influence of internal erosion on soil strength is experimentally studied through a series of one-dimensional upward seepage tests at constant water head and cone penetration tests. By giving upward seepage flow to the gap-graded soil specimens, internally eroded soils are

created. Mechanical consequences of internal erosion are examined by cone penetration test on internally eroded specimens.

Before internal erosion, the relationship between average hydraulic gradient and flow velocity is basically linear. After the onset of erosion, the slope of the relationship is no longer linear, indicating that the hydraulic conductivity of soils drastically increases with progress of the internal erosion. The hydraulic gradient for internal erosion is found to be about one fifth to one third of the critical hydraulic gradient for soil stability. The less the fine content, the larger the hydraulic gradient required to cause internal erosion. Those specimens containing the same mass ratio of fines with larger relative density requires a larger critical hydraulic gradient to initiate internal erosion. The fine particle loss proportionally increases with the imposed hydraulic gradient.

The internal erosion causes cone tip resistance reduction, the extent of which may be related with the imposed hydraulic gradient. A larger imposed hydraulic gradient, indicating the more the fine particle loss would lead to the further cone resistance reduction. Drastic change in the strength can be seen with the hydraulic gradient over 0.5. The internal erosion causes the angle of shearing resistance of a soil specimen decrease within certain hydraulic gradient range.

**REFERENCE:**

1) Al-Awkati, Z.A. (1975): On problems of soil bearing capacity at depth, PhD thesis, Department of Civil Engineering, Duke University, Durham, NC.

2) Been, K., et al (1986): The cone penetration test in sands: Part 1, state parameter interpretation. Geotechnique, Vol.36, No.2, 239~249.

3) Been, K., et al (1987): The cone penetration test in sands: Part 2, general inference of state. Geotechnique, Vol.37, No.3, 285~299.

4) Bradshaw, A.S. and Baxter, C.D. (2007): Sample preparation of silts for liquefaction testing. Geotechnical Testing Journal, Vol.30, No.4, 324~332.

5) Burenkova, V.V. (1993): Assessment of suffusion in non-cohesive and graded soils. Filters in Geotechnical and Hydraulic Engineering, Brauns, Heibaum & Schuler, Balkema, Rotterdam, 357~360.

6) Durgunoglu, H.T. and Mitchell, J.K. (1975): Static penetration resistance of soils: I-ANALYSIS. Proceedings, ASCE Specialty Conference on in-situ Measurement of Soil Parameters, Raleigh, Vol.1.

7) Frost, J.D. and Park, J.Y. (2003): A critical assessment of the moist tamping technique. Geotechnical Testing Journal, Vol.26, No.1, 57~69.

8) Gui, M.W. and Bolton, M.D. (1998): Geometry and scale effects in CPT and pile design. Geotechnical site characterization, Robertson & Mayne, 1063~1068.

9) Istomina, V.S. (1957): Filtration stability of soils. Gostroizdat, Moscow, Leningrad.

10) Janbu, N. and Senneset, K. (1974): Effective stress interpretation of in situ static penetration tests. Proceedings of the European Symposium on Penetration Testing, ESOPT I, Stockholm, Sweden, Vol. 2.2, 181~193.

11) Kenney, T.C. and Lau, D. (1985): Internal stability of granular filters. Can. Geotech. J, Vol.22, 215~225.

12) Kenney, T.C. and Lau, D. (1986): Internal stability of granular filters. Can. Geotech. J, Vol.23, 420~423.

13) Ladd, R.S. (1978): Preparing test specimens using undercompaction. Geotechnical Testing Journal, Vol.1, No.1, 16~23.

14) Mao, C.X. (2005): Study on piping and filters: part 1of piping. Rock and Soil Mechanics, Vol.26, No.2, 209~215. (in Chinese)

15) Mayne, P.W. (1991): Determination of OCR in Clays by Piezocone Tests using cavity expansion and critical state concepts. Soils and Foundations, Vol.31, No.2, 65~76.

16) Mitchell, J.K. (1976): Fundamentals of soil behavior. New York: Wiley.

17) Moffat, R.A. and Fannin, R.J. (2006): A large permeameter for study of internal stability in cohesionless soils. Geotechnical Testing Journal, Vol.29, No.4, 273~279.

18) Omine, K. and Ochiai, H. (1992): Stress-strain relationship of mixtures with two different materials and its application to one-dimensional compression property of sand-clay mixed soils. Proceedings of Japan Society of Civil Engineers, No.448/III-19, 121~130. (in Japanese)

19) Omine, K., Ochiai, H. and Yasufuku, N. (1996): Evaluation of strength-deformation properties of Light-weight soils based on two-phase mixture model. Proceedings of Twelfth Southeast Asian Geotechnical Conference, Kuala Lumpur, 101~106.

20) Schnaid, F. and Houlsby, G.T. (1991): An assessment of chamber size effects in the calibration of in situ tests in sand. Geotechnique, Vol.41, No.3, 437~445.

21) Skempton, A.W. and Brogan, J.M. (1994): Experiments on piping in sandy gravels. Geotechnique, Vol.44, No.3, 449~460.

22) Terzaghi, K. and Peck, R.B. (1948) Soil Mechanics in Engineering practice. 1st.Edition. John Wiley and Sons, New York.

23) Terzaghi, K., Peck, R.B. and Mesri, G. (1996) Soil Mechanics in Engineering practice. 3rd.Edition. John Wiley and Sons, INC.

24) Thevanayagam, S. and Mohan, S. (2000): Intergranular state variables and stress-strain behavior of silty sands. Geotechnique, Vol.50, No.1, 1~23.

25) Tomlinson, S.S. and Vaid, Y.P. (2000): Seepage forces and confining pressure effects on piping erosion. Can. Geotech. J., Vol.37, 1~13.

26) U.S. Army Corps of Engineers (1953): Filter experiments and design criteria. Technical Memorandum No. 3~360, Waterways Experiment Station, Vicksburg.

27) Vallejo, L.E. (2001): Interpretation of the limits in shear strength in binary granular mixtures. Can. Geotech. J., Vol.38, 1097~1104.

28) Vesic, A.S. (1972): Expansion of cavities in infinite soil masses. ASCE Journal of the Soil Mechanics and Foundations Dvision, 96(SM3), 265~290.

29) Wan, C.F. (2006): Experimental investigations of piping erosion and suffusion of soils in embankment dams and their foundations, PhD thesis, School of Civil and Environmental Engineering, University of New South Wales.

30) Yang, Z.X., Li, X.S. and Yang, J. (2008): Quantifying and modeling fabric anisotropy of granular soils. Geotechnique, Vol.58, No.4, 237~248.

APPENDIX:

## SIZE EFFECTS IN CPT TESTS

*Particle size effect*

Due to the comparatively large particle size of Silica No.3, the particle size effect, characterized by the ratio of cone diameter to mean particle size, should be considered. Gui and Bolton (1998) introduced the new concept “effective diameter”, which is the sum of cone diameter and mean particle size, to erase the particle size effect. The effective diameter was considered in the interpretation of the test data in this study. The mean particle size was obtained from the particle size distribution curve before and after the seepage test.

*Chamber size effect*

Chamber size and imposed boundary conditions are influential on cone resistance. Detailed discussions can be found in Been, et al (1986, 1987), Mayne (1991), Schnaid and Houlsby (1991) and among others. Even though many studies have been conducted on this issue, it appears that there are no universally accepted explanations. Generally, the chamber size effect is less for loose sand, while for medium and dense sand, the size effect depends on chamber-to-cone diameter ratio or stress state and so on.

To assess the size effect, the CPT tests were conducted using a 300mm diameter container with the diameter ratio of 30 as well as the seepage cell with the diameter ratio of 10. The dry Silica No.3 specimen is prepared in the abovementioned two containers by the air pluviation method. Three relative densities corresponding to loose (Dr = 30%), medium (Dr = 70%) and dense (Dr = 100%) states are considered. In terms of Bearing Capacity Number $N_q$, the container diameter effect is plotted in Fig. A1. As expected, the size effect becomes much more obvious with the larger relative density. Due to the comparatively small relative densities of the tested specimens in the tests, this effect was not considered in the interpretation of the test data in this study.

# Tables:

**Table 1 Sand particle size distribution parameters**

| Property | Silica No.3 | Silica No.8 |
|---|---|---|
| Median particle size $D_{50}$ (mm) | 1.72 | 0.16 |
| Effective particle size $D_{10}$ (mm) | 1.37 | 0.087 |
| Uniformity Coefficient $C_u$ | 1.29 | 2.09 |
| Curvature Coefficient $C_c$ | 0.99 | 2.34 |

**Table 2 Specific gravity, Maximum void ratio, Minimum void ratio and permeability of Silica sand**

| | | Silica No.3 | Silica No.8 |
|---|---|---|---|
| Specific gravity | | 2.63 | 2.63 |
| Maximum void ratio ($e_{max}$) | | 1.009 | 1.333 |
| Minimum void ratio ($e_{min}$) | | 0.697 | 0.703 |
| Hydraulic conductivity (m/s) | 30%* | $6.6\times10^{-3}$ | $3.4\times10^{-5}$ |
| | 60%* | $5.6\times10^{-3}$ | $2.6\times10^{-5}$ |
| | 80%* | $4.9\times10^{-3}$ | $2.1\times10^{-5}$ |

* Relative density

**Table 3 Sand parameters of the four specimens**

| Specimen No. | A | B | C | D |
|---|---|---|---|---|
| Specific gravity | 2.63 | 2.63 | 2.63 | 2.63 |
| Maximum void ratio | 0.756 | 0.764 | 0.775 | 0.795 |
| Minimum void ratio | 0.367 | 0.373 | 0.385 | 0.402 |
| Void ratio range* | 0.389 | 0.391 | 0.39 | 0.393 |

* The difference in the void ratio between loosest and densest sand states

**Table 4 Assessment of specimens' vulnerability to internal by current methods**

| | The methods used to assess of internal stability | | | | |
|---|---|---|---|---|---|
| | U.S.Army (1953) | Istomina (1957) | Kenney & Lau (1986) | Burenkova (1993) | Mao (2005) |
| A | S | S | U | U | U |
| B | S | S | U | U | U |
| C | S | S | U | U | U |
| D | U | U | U | U | U |

Note: "U" means Unstable; "S" means Stable

**Table 5 Seepage test specimens**

| Sample No. | Fine particle content (%) | Relative density (%) | Void ratio |
|---|---|---|---|
| A-30 | 25 | 30 | 0.63 |
| A-60 | 25 | 60 | 0.51 |
| B-20 | 20 | 20 | 0.69 |
| B-60 | 20 | 60 | 0.53 |
| C-20 | 16.7 | 20 | 0.70 |
| C-60 | 16.7 | 60 | 0.54 |
| D-30 | 14.3 | 30 | 0.69 |
| D-60 | 14.3 | 60 | 0.58 |

**Table 6 Fine particle loss at different depth of SpecimenA-60**

| Zone / Max. Hydraulic gradient | | A | B | C |
|---|---|---|---|---|
| Particle loss (%) | 0.45 | 3.00 | 2.70 | 4.10 |
| | 0.51 | 3.00 | 2.94 | 5.11 |

**Table 7 Number of specimens undertaken by CPT**

| Specimen No. | Before internal erosion | After internal erosion |
|---|---|---|
| A-30 | 1 test | 1 test |
| A-60 | 1 test | 3 tests* |
| B-20 | 1 test | 1 test |
| B-60 | 1 test | 2 tests* |
| C-20 | 1 test | 1 test |
| C-60 | 1 test | 2 tests* |
| D-30 | 1 test | ---------- |
| D-60 | 1 test | 1 test |

* For the dense specimens, seepage tests ended at different imposed hydraulic gradients were performed.

**Table 8 Details of tested specimens in calibration studies**

| Specimens | Relative Density (%) | Void ratio | Mineralogy | Shape | Bearing capacity number |
|---|---|---|---|---|---|
| Silica No.3 | 20 | 0.95 | Mainly quartz | Subangular | 26 |
| Silica No.3 | 60 | 0.82 | Mainly quartz | Subangular | 84 |
| Silica No.3 | 100 | 0.70 | Mainly quartz | Subangular | 938 |
| Specimen A | 60 | 0.51 | Mainly quartz | Subangular | 508 |
| Specimen B | 60 | 0.53 | Mainly quartz | Subangular | 609 |
| Specimen C | 60 | 0.54 | Mainly quartz | Subangular | 722 |
| Specimen D | 60 | 0.58 | Mainly quartz | Subangular | 1072 |

**Table 9 Summary of soil strength change due to internal erosion**

| | Normalized bearing capacity number | Angle of shearing resistance (°) | | Strength reduction, $\Delta R$ (%) | Max. imposed hydraulic gradient |
|---|---|---|---|---|---|
| | | Before internal erosion | After internal erosion | | |
| SpecimenA-30 | 0.86 | 36.1 | 35.8 | 1.0 | 0.22 |
| SpecimenB-20 | 0.96 | 32.7 | 32.6 | 0.3 | 0.25 |
| SpecimenC-20 | 0.95 | 35.1 | 35.0 | 0.3 | 0.24 |
| SpecimenA-60 | 0.33 | 41.1 | 39.5 | 6.1 | 0.54 |
| SpecimenB-60 | 0.78 | 41.6 | 41.2 | 1.4 | 0.41 |
| SpecimenC-60 | 0.71 | 42.1 | 41.6 | 1.8 | 0.38 |
| SpecimenD-60 | 0.67 | 42.4 | 41.8 | 2.1 | 0.28 |

Figures:

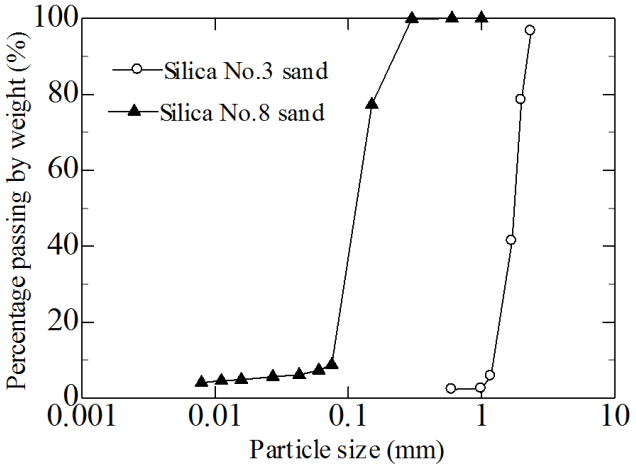


**Fig.1 Particle size distribution curves of Silica No.3 and No.8**

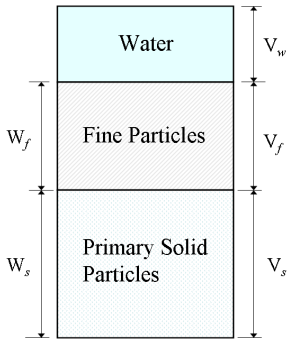


Symbols mean:
$V_s$: Coarse particles volume forming the primary fabric of soil;
$V_f$: Erodible fine particles volume filling inside the voids between coarse particles;
$V_w$: Volume of water;
$W_s$: Coarse particles weight;
$W_f$: Erodible fine particles weight.

**Fig.2 Schematic Phase Diagrams of saturated binary soil**

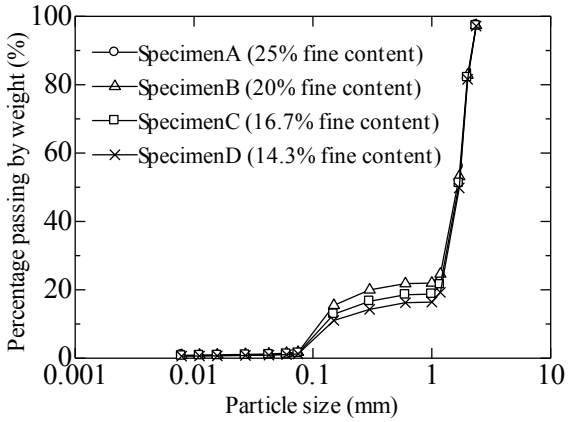


**Fig.3 Particle size distributions of four soils**

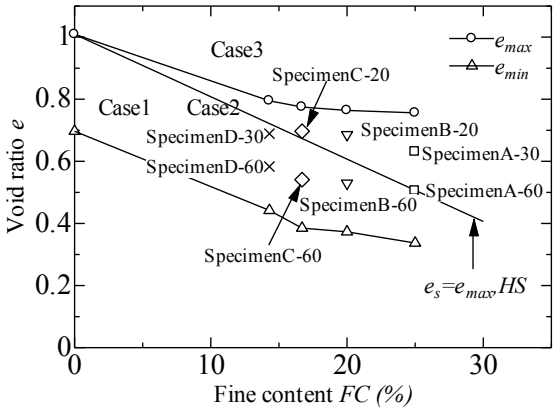


**Fig.4 Intergranular matrix phase diagram**

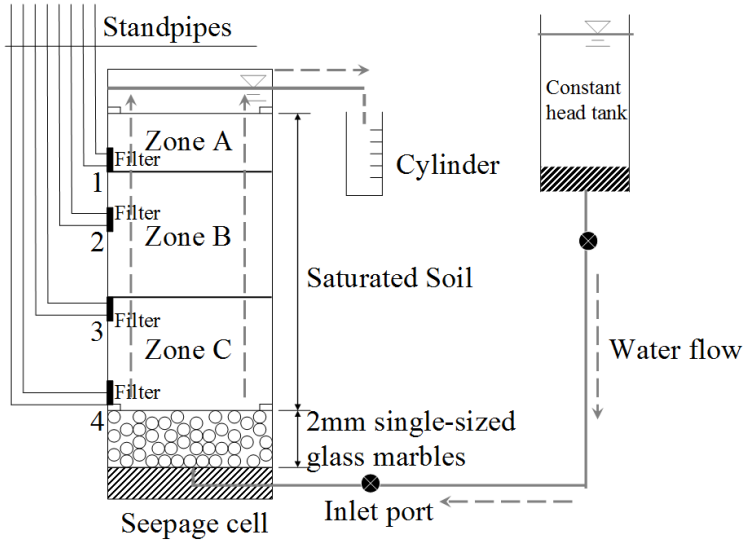


**Fig.5 Schematic diagram of the seepage test assembly**

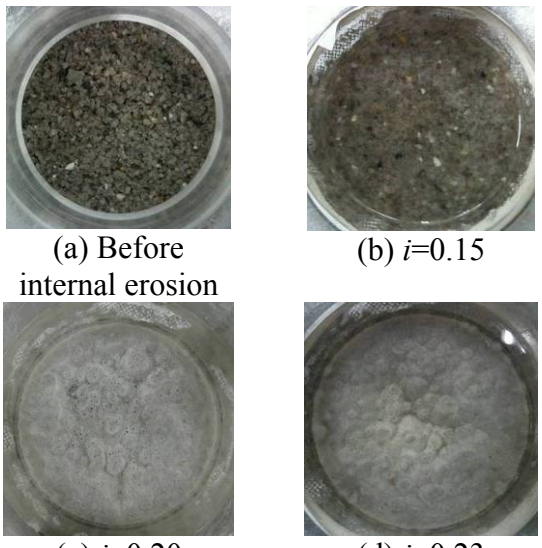

(a) Before internal erosion (b) *i*=0.15

(c) *i*=0.20 (d) *i*=0.23

**Fig.6 Observed particle migrations from top (Specimen A-30)**

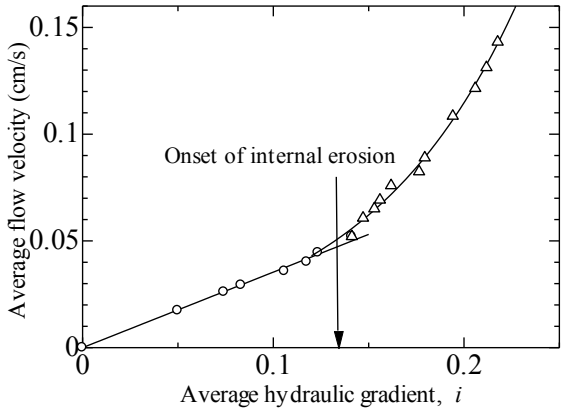


**Fig.7 Hydraulic gradient and flow velocity relation (Specimen A-30)**

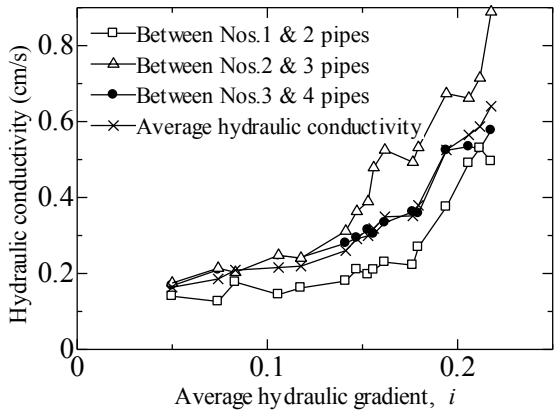


**Fig.8 Local hydraulic conductivity variance (Specimen A-30)**

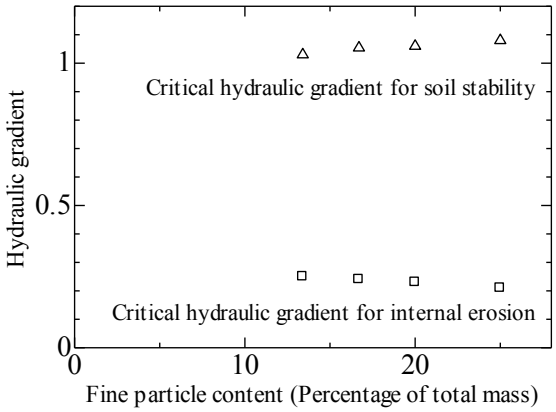


**Fig.9 Relation between fine content and $i_s$, $i_c$ for dense samples**

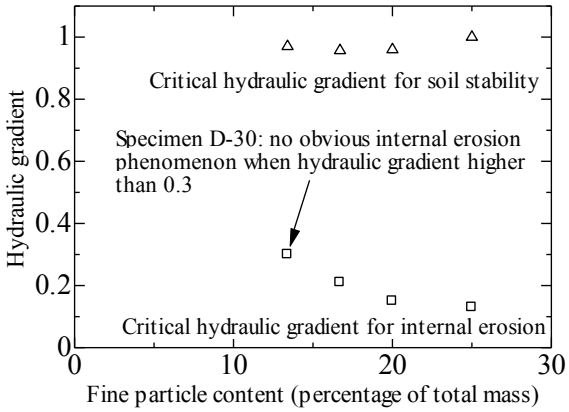


**Fig.10 Relation between fine content and $i_s$, $i_c$ for loose samples**

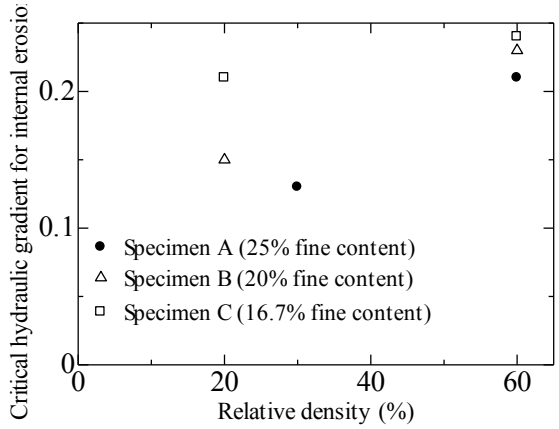


**Fig.11 Relationship between relative density and $i_s$**

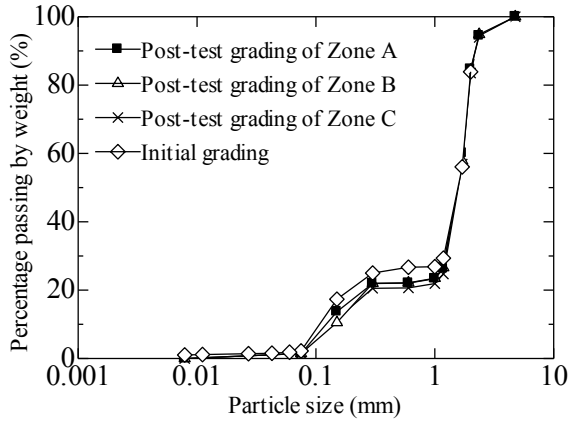


**Fig.12 Particle size distribution curve along the depth**

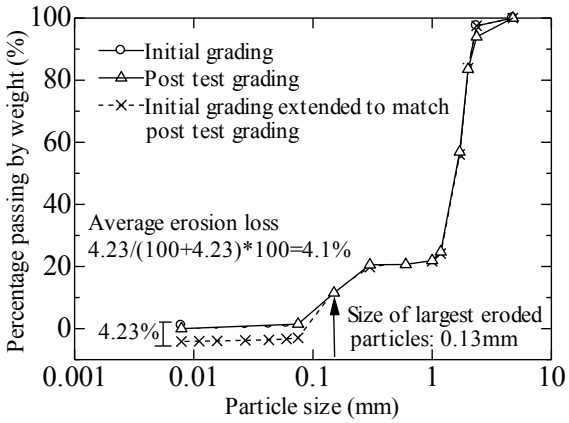


**Fig.13 Graphical method of fine particle loss assessment**

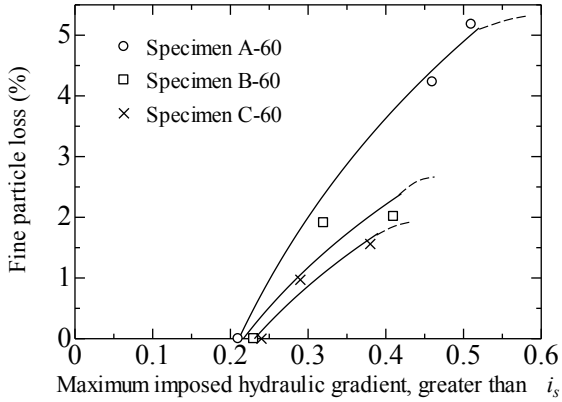


**Fig.14 Fine particle loss variance with the maximum imposed hydraulic gradient at various fine contents**

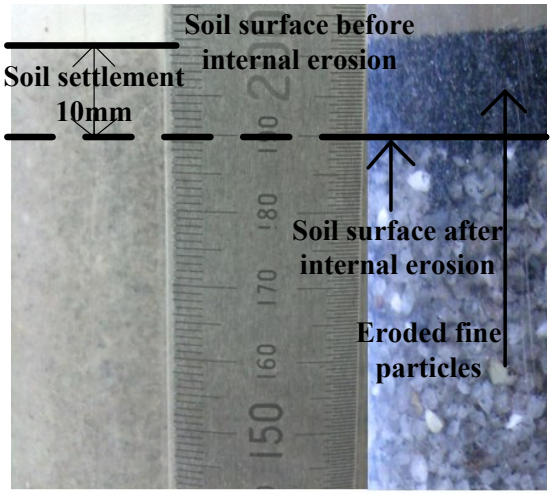


**Fig.15 Soil volume change due to internal erosion (Specimen A-60)**

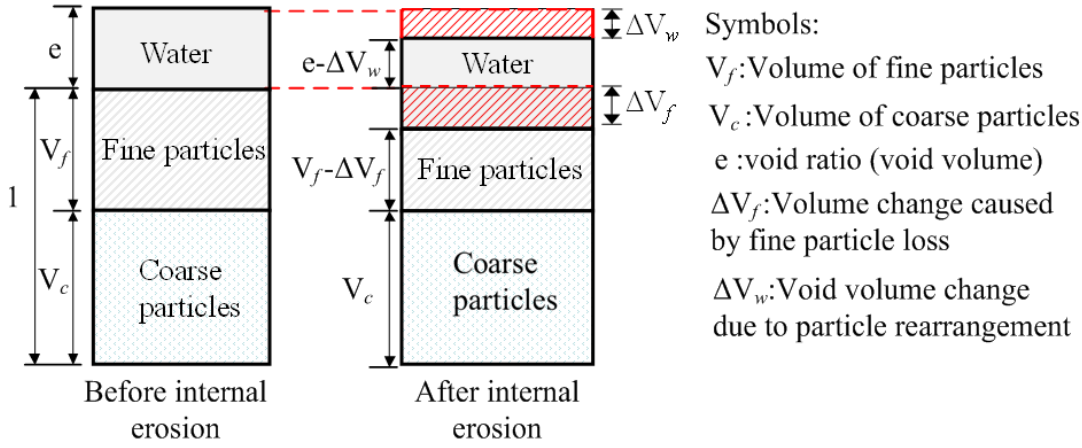


**Fig.16 Specimen possible volumetric deformation**

**Fig.17 Miniature Cone penetrometer**

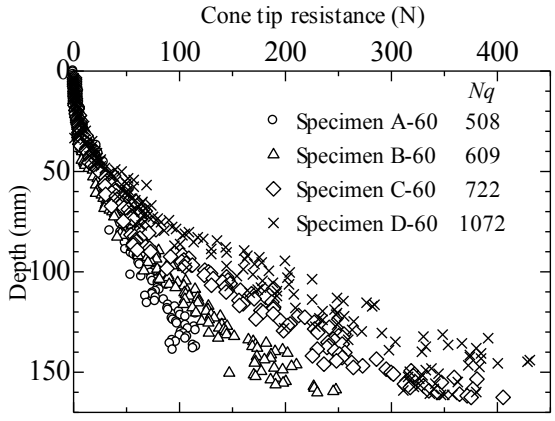


**Fig.18 Cone resistance of the dense specimens**

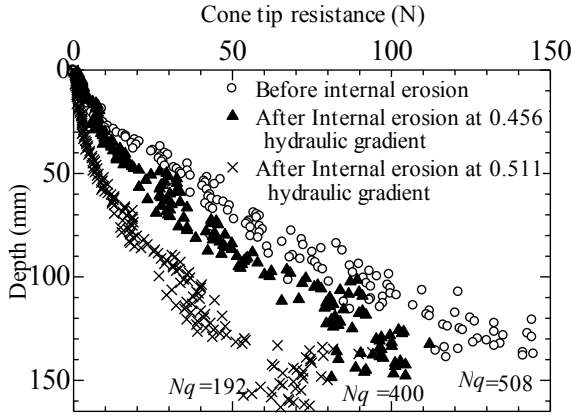


**Fig.19 Cone resistance before and after internal erosion (Specimen A-60)**

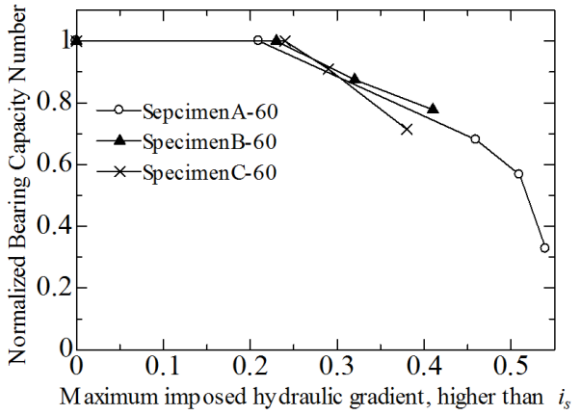


**Fig.20 Maximum imposed hydraulic gradient and normalized Bearing Capacity Number relation**

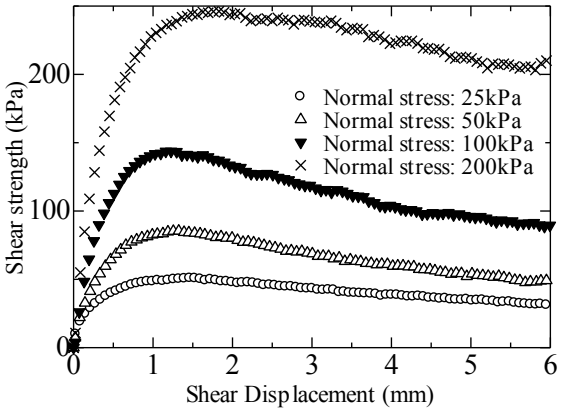


**Fig.21 Shearing Displacement and Strength relationship (Specimen A-60)**

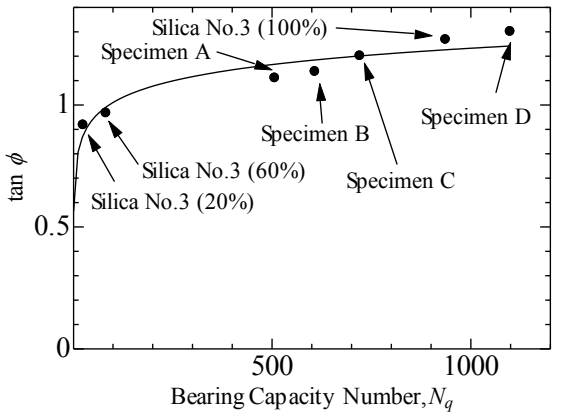


**Fig.22 Relationship between bearing capacity number and tan$\phi$**

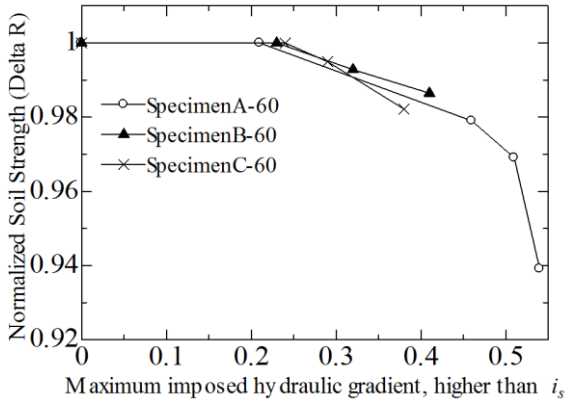


**Fig.23 Maximum imposed hydraulic gradient and normalized soil strength relation**

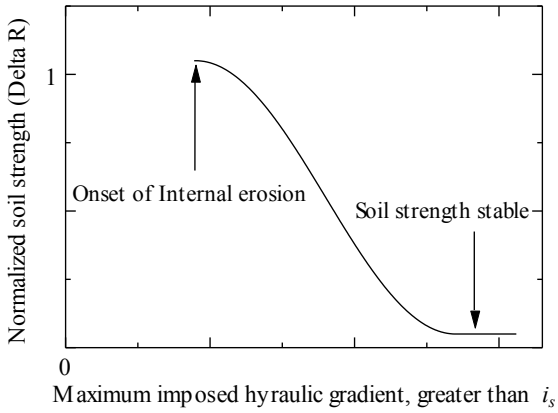


**Fig.24 Possible strength reduction curve against maximum imposed hydraulic gradient**

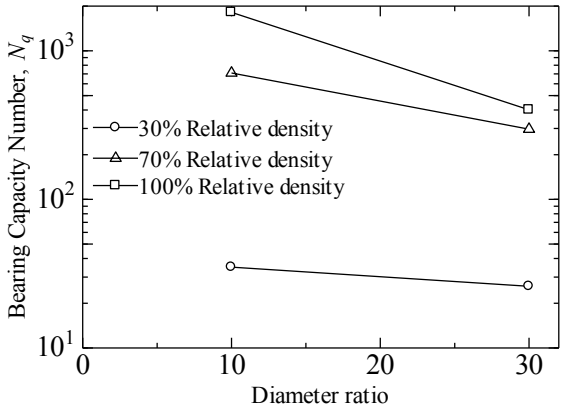


**Fig.A1 Relationship between bearing capacity number and diameter ratio**